Cancer Research

Phosphorescent Light–Emitting Iridium Complexes Serve as a Hypoxia-Sensing Probe for Tumor Imaging in Living Animals

Shaojuan Zhang[1], Masahiro Hosaka[1], Toshitada Yoshihara[3], Kazuya Negishi[3], Yasuhiko Iida[2], Seiji Tobita[3], and Toshiyuki Takeuchi[1]

Abstract

Iridium complex is a promising organic light–emitting diode material for next generation video displays that emits phosphorescence quenched by oxygen. We used this oxygen-quenching feature for imaging tumor hypoxia. Red light–emitting $Ir(btp)_2(acac)$ (BTP) presented hypoxia-dependent light emission in culture cell lines, whose intensity was in parallel with hypoxia-inducible factor-1α images. BTP was further applied to imaging five nude mouse transplanted with tumors. All tumors presented a bright BTP-emitting image even 5 minutes after injection. The minimal image recognition size was ~2 mm in diameter. By morphologic examination and phosphorescence lifetime measurement, BTP appeared to localize to the tumor cells. Because BTP is easily modifiable, we synthesized BTP analogues with a longer excitation/emission wavelength. One of them, BTPHSA, depicted clear imaging from tumors transplanted 6 to 7 mm deep from the skin surface. We suggest that iridium complex materials have a vast potential for imaging hypoxic lesions such as tumor tissues. *Cancer Res; 70(11); 4490–8. ©2010 AACR.*

Introduction

Hypoxia is highly notable in tumor tissues (1, 2), in which hypoxia-inducible factor (HIF)-1α is induced by inhibiting its degradation through the decrease in oxygen-sensing prolyl 4-hydroxylase activity (3, 4). HIF-1α regulates a variety of gene expressions including vascular endothelial growth factor (VEGF) and glucose transporter (Glut)-1. Through HIF-1α–mediated gene expression, tumors are vascularized by VEGF to receive oxygen and nutrients for their growth in a hypoxic milieu (2). Several hypoxia-associated probes have been developed for tumor imaging including nitroimidazole (5, 6), Cu-diacetyl-bis(N^4-methylthiosemicarbazone (7), and fluorodeoxyglucose (8). They are used with radioisotope for visualization by positron emission tomography (PET).

An optical method was shown to directly detect oxygen in cells and tissues by using oxygen-dependent quenching of phosphorescence (9). For this purpose, two groups of phosphorescent probes were developed: one is ruthenium(II) complexes and iridium(III) complexes (10–12), and the other is metalloporphyrin complexes (13–15). The difference of the two groups is primarily attributed to the phosphorescence lifetime, which is shorter for the former than for the latter. As an oxygen sensor, metalloporphyrins are too sensitive to oxygen quenching because of their long phosphorescence lifetime. Therefore, they have been modified by decorating "molecular coats" to adjust oxygen access to core porphyrins (14, 16, 17). Furthermore, the molecular coats can protect the phosphor from albumin and give them their hydrophilic nature. However, their molecular size enlarges to over 2,000 Da exemplified by the paradium-porphyrin complex (13, 14). Ruthenium(II) complex and iridium(III) complex were also used with binding to polymer or quantum dots (12, 18). These large probes have been applied to measure oxygen pressure in microcapillary vessels (13, 14, 16).

Iridium complexes possess highly phosphorescent and photostable properties that are required for use as organic light–emitting diode emitters. Furthermore, we are able to use various ligands to improve the photophysical and chemical properties for hypoxic tissue imaging. Because iridium complexes are relatively small in molecular size (600–800 Da) and lipophilic if not modified, they may be able to cross the cell membrane and measure intracellular oxygen pressure. In this study, we first used the red-emitting iridium complex $Ir(btp)_2(acac)$ [BTP; bis(2-(2′-benzothienyl)-pyridinato-N,$C^{3'}$)iridium(acetylacetonate); Fig. 1A; ref. 19). The red phosphorescence is advantageous for tissue penetrance and its moderately long lifetime (5.8 μs) is favorable for oxygen-induced quenching. Based on these properties, we applied this phosphor for hypoxic tumor imaging without binding to any carriers. Because the excitation and emission

Authors' Affiliations: [1]Secretion Biology Laboratory, Institute for Molecular and Cellular Regulation and [2]Division of Diagnostic Radiology and Nuclear Medicine, Graduate School of Medical Sciences, Gunma University, Maebashi, Japan; and [3]Department of Chemistry and Chemical Biology, Graduate School of Engineering, Gunma University, Kiryu, Japan

Note: Supplementary data for this article are available at Cancer Research Online (http://cancerres.aacrjournals.org/).

S. Zhang, M. Hosaka, and T. Yoshihara contributed equally to this work.

Corresponding Author: Toshiyuki Takeuchi, Secretion Biology Laboratory, Institute for Molecular and Cellular Regulation, Gunma University, Showa-machi, Maebashi 371-8512, Japan. Phone: 81-272-20-8855; Fax: 81-272-20-8896; E-mail: tstake@showa.gunma-u.ac.jp.

doi: 10.1158/0008-5472.CAN-09-3948

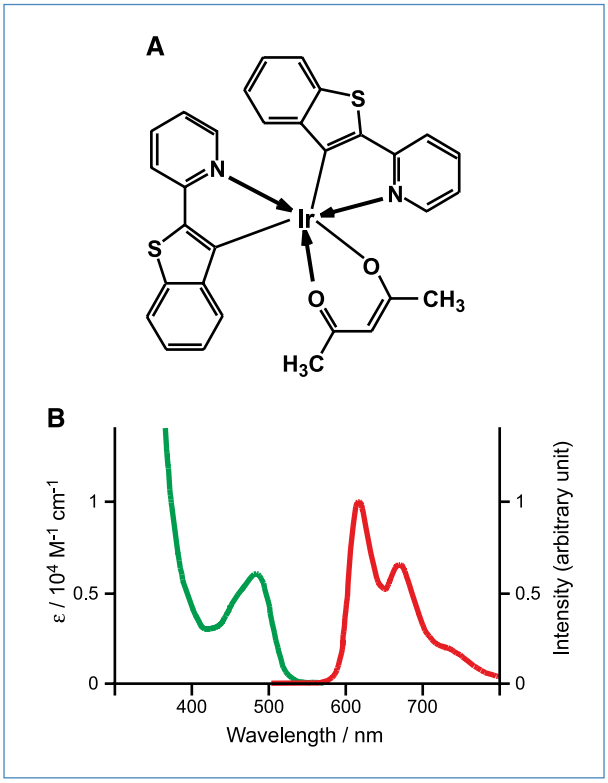

Figure 1. Spectral properties of BTP. A, chemical structure of $Ir(btp)_2$ (acac). B, absorption (green line) and phosphorescence (red line) spectra of BTP in DCE at room temperature.

wavelengths of BTP do not reach the near IR zone, we shifted them to a much longer zone by modification. We found that this iridium complex is easily modified for more desirable phosphorescent probes.

Materials and Methods

Physicochemical features of iridium complex

BTP was synthesized from $IrCl_3 \cdot 3H_2O$ (Kanto) according to the procedure found in the literature (19). A mixture of 2-(benzo[*b*]thiophen-2-yl)pyridine (460 mg, 2.2 mmol), $IrCl_3 \cdot 3H_2O$ (390 mg, 1 mmol), 2-ethoxyethanol (30 mL), and distilled water (10 mL) was heated at reflux for 15 hours. After cooling, the precipitate formed was filtered to give a chloro-bridged dimer and washed thoroughly with methanol and *n*-hexane. To the mixture of the chloro-bridged dimer (260 mg, 0.2 mmol) and Na_2CO_3 (170 mg, 1.6 mmol), 2-methoxyethanol (30 mL) and acetyl acetone (1.0 mL, 9.5 mmol) were added and then the slurry was refluxed for 2 hours. After the mixture was cooled down, the precipitate formed was collected by filtration and washed thoroughly with methanol and *n*-hexane. Yield was as follows: 180 mg (62%). ^1H NMR (300 MHz, $CDCl_3$) δ: 8.43 (d, 2H, J = 5.4 Hz), 7.77 (t, 2H, J = 8.4 Hz), 7.63 (d, 4H, J = 7.2 Hz), 7.07-6.99 (m, 4H), 6.80 (t, 2H, J = 7.8), 6.20 (d, 2H, J = 8.1 Hz), 5.26 (s, 1H), 1.78 (s, 6H).

Dimyristoyl-L-α-phosphatidylcholine (DMPC; Sigma 99%) was used for lipid membrane and liposome preparation. 1,2-Dichloroethane (DCE; Kishida, spectroscopic grade) and *n*-hexane (Kanto; fluorometric grade) were used without further purification. Deionized water was purified by using Millipore (MILLI-Q-LABO). Small unilamellar vesicles were prepared by using the ethanol injection method. The ethanolic solution of DMPC (3.0×10^{-2} moldm^{-3}, 0.1 mL) was injected rapidly into Tris-HCl buffer (2.85 mL; pH 7.0) at 50°C. The incorporation of BTP into the small unilamellar vesicles was carried out by adding a stock solution of BTP (6.0×10^{-4} moldm^{-3}, 0.05 mL) in DMSO. The final concentration of the BTP probe was 1.0×10^{-5} moldm^{-3}. The solution was equilibrated for 1 hour above the phase transition temperature (23°C) of DMPC.

Human serum albumin (HSA; 96–99%) was purchased from Sigma. HSA solution in Tris-HCl buffer (pH 7.0) was bubbled with oxygen-nitrogen mixed gas to adjust the dissolved oxygen concentration and then a small amount of BTP solution in DMSO was added to the HSA solution. Final concentrations of BTP and HSA in Tris buffer/DMSO (98: 2, v/v) were 5 and 200 μmol/L, respectively. Oxygen-quenching experiments were carried out for BTP dissolved in a bulk solution, DMPC membrane–incorporated BTP, and HSA-bound BTP. Nitrogen-oxygen mixed gas regulated with a mass-flow meter (HORIBA STEC; SEC-V110DM, PAC-D2) was bubbled through the sample solution for 20 minutes before luminescence measurement.

Absorption and emission spectra were measured with a UV/vis spectrophotometer (Jasco, Ubest-V550) and a spectrofluorimeter (Hitachi, F-4010), respectively. The emission spectrum was corrected for spectral sensitivity. Phosphorescence lifetime was measured with a time-correlated single-photon counting fluorimeter (Edinburgh Analytic Instrument, FL-900CDT). A nanosecond-pulsed discharge lamp (pulse width, ~1.0 ns; repetition rate, 40 kHz) filled with nitrogen gas was used for an excitation light source.

Cell culture and BTP uptake

We used four cell lines, human uterine cancer–derived HeLa, Chinese hamster ovary (CHO)–derived CHO, mouse oral squamous carcinoma–derived SCC-7, and human glioma–derived U251. We also used O_2 concentration–changeable multigas incubator MCO-5M (Sanyo). Cells were cultured in DMEM (Invitrogen) with 10% fetal bovine serum (FBS) at 37°C. The cells were cultured under four O_2 concentrations: 2.5, 5.0, 10, and 20% for 24 hours at 37°C. Then, BTP was added to the medium at a final concentration of 50 μmol/L for 1 hour for visualization (520–550 nm excitation/over 580 nm emission).

Tumor transplantation to nude mice

We conducted our animal experiments in accordance with the guidelines for the Care and Use of Laboratory Animals of the Medical Research Council of Gunma University. Tumor transplants were established in female athymic nude mice by injection of 5×10^6 SCC-7, human glioma–derived U87, human lymphoma–derived RAMOS, human colon carcinoma–derived HT-29, and mouse lung cancer–derived LL-2. Experiments with tumor-bearing mice were performed 2 weeks after the injection of tumor cells. To transplant

tumors on the liver surface, tumors with an ~1 mm^3 size were adhered one by one on the surface by a surgical glue (Aron α A, Sankyo Pharma).

In vivo imaging

Luminescence images of a whole mouse body and close-up image were obtained using the Maestro FL500 *in vivo* imaging system (CRi, Inc.). A band-pass filter from 520 to 550 nm and a long-pass filter over 580 nm were used for excitation and emission light, respectively. The tunable filter was automatically stepped in 10-nm increments from 550 to 800 nm, whereas the camera captured images at each wavelength interval with 1,500 ms exposure. Spectral fluorescence images consisting of autofluorescence spectra and BTP spectra were obtained and then unmixed, based on their spectral patterns using commercial software (Maestro software, CRi, Inc.). The spectra for unmixed images are shown in Fig. 3 (blue and sky-blue are auto-fluorescence; red is BTP spectra). The intensities of the BTP signal were automatically calculated with unmixed images by the Maestro software.

Measurement of oxygen partial pressure

pO_2 in the tumors was measured with a needle-type polarographic oxygen electrode (PO2-150S, Eikou-kagaku Co. Ltd.). An oxygen electrode probe of a 200 μm diameter was inserted into tumors of immobilized mice without general anesthesia; then pO_2 was measured at 10 or more different points in each tumor; and the mean pO_2 was calculated. After the measurements, the tumors were excised and weighed.

BTP localization in tissues

The Olympus IV100 microscope was used for imaging BTP signals in tissues. Images were acquired with the IV100 imaging software (Olympus). A 488-nm argon laser and 586 to 615 nm band-pass filters were used for the excitation and emission of BTP. AngioSense 750 (VisEn Medical) was used to visualize blood vessels. A 748-nm laser and 770 nm long-pass filters were used for the excitation and emission of AngioSense 750.

In vivo lifetime measurement

In vivo phosphorescence lifetime measurement was performed for SCC-7 tumor–bearing mice with a time-correlated single photon counting fluorimeter. The excitation light (337 nm) from a nanosecond pulsed discharge lamp filled with nitrogen gas was collimated to the tumor area or normal tissues in each mouse after removing a part of the back skin and the phosphorescence at 620 nm was detected by a photomultiplier tube after passing through a monochromator.

Results

Photophysical properties of BTP complexes

To examine BTP phosphor quenching, we assumed two situations because of its lipophilic nature (Fig. 1A): BTP in the lipid bilayer membrane and BTP bound to blood components exemplified by albumin. To test the first assumption, we measured its uptake into an artificial membrane composed of DMPC (1 mmol/L). Indeed, over 98% of BTP (10 μmol/L) was partitioned into the membrane at 35°C. We then investigated the photophysical properties of BTP in DMPC liposome and in DCE and *n*-hexane solutions. BTP in a deaerated DCE solution showed the first absorption maximum at 483 nm with a molar absorption coefficient of 6,100 $M^{-1}cm^{-1}$ and it showed intense phosphorescence at 616 nm (Fig. 1B). The phosphorescence quantum yield (Φ_p^0) and lifetime (τ_p^0) in a deaerated DCE solution (oxygen partial pressure pO_2 is assumed to be 0) were 0.32 and 5.8 μs, respectively, at room temperature. The phosphorescence quenching due to dissolved oxygen in solution or membrane can be examined by the following Stern-Volmer equation:

$$\frac{\Phi_p^0}{\Phi_p} = \frac{\tau_p^0}{\tau_p} = 1 + k_q \tau_p^0 pO_2,$$

in which Φ_p and τ_p, respectively, are the phosphorescence quantum yield and lifetime, and k_q is a bimolecular quenching rate constant (20). At 35°C, the k_q in *n*-hexane was 5.7×10^4 $mmHg^{-1}s^{-1}$ and 1.2×10^4 $mmHg^{-1}s^{-1}$ in the DMPC membrane. When τ_p^0 = 5.3 μs (DMPC membrane) and tissue pO_2 = 60 mmHg are applied to this equation with the assumption that the quenching rate constants in the membrane and tissue are equal, Φ_p^0/Φ_p comes to 4.8, indicating that BTP phosphorescence is quenched in the tissue pO_2 milieu of 60 mmHg. Because tissue pO_2 = 60 mmHg is not hypoxic (7), BTP is presumed to become phosphorescent at lower pO_2, so BTP seems to be applicable to hypoxic tissue pO_2 estimation.

To test the second assumption that BTP is bound to albumin, we measured the oxygen-induced quenching rate constant (k_q) of the phosphorescence bound to albumin (200 μmol/L) in Tris-buffer/DMSO (98:2 v/v) solution at 35°C. Based on the Stern-Volmer analyses, the k_q was obtained as 5.0×10^2 $mmHg^{-1}s^1$ along with τ_p^0 = 4.3 μs (pO_2 = 0 mmHg) and τ_p = 3.2 μs (pO_2 = 158 mmHg), which was in fact much smaller than that (1.2×10^4 $mmHg^{-1}s^{-1}$) in the DMPC membrane. Thus, BTP phosphorescence is barely changeable between hypoxic and normoxic conditions in the presence of albumin, indicating that BTP is not efficient for oxygen quenching when it binds to albumin.

BTP to culture cells in a hypoxic milieu

We examined oxygen quenching in culture cells in a physiologic pO_2 milieu. If BTP binds to albumin in the culture medium and remains there without passing through the cell membrane, the cells would not emit enough phosphorescence. We placed four cell lines, human uterine cancer–derived HeLa, CHO-derived CHO, mouse oral squamous carcinoma–derived SCC-7, and human glioma–derived U251 in a 20% O_2 culture condition. In normoxia, the three cell lines did not exhibit notable phosphorescence with BTP (50 μmol/L; Fig. 2A). To the contrary, they emitted bright red phosphorescence in a 5% O_2 culture. We then observed the BTP phosphorescence in decreasing O_2 levels from 20% to 2.5% using SCC-7 cells (Fig. 2B, top). With a decrease in O_2 concentration, the phosphorescence increased in an inverted manner. Likewise, HIF-1α was increasingly immunostained with a decrease in O_2 levels and appeared to

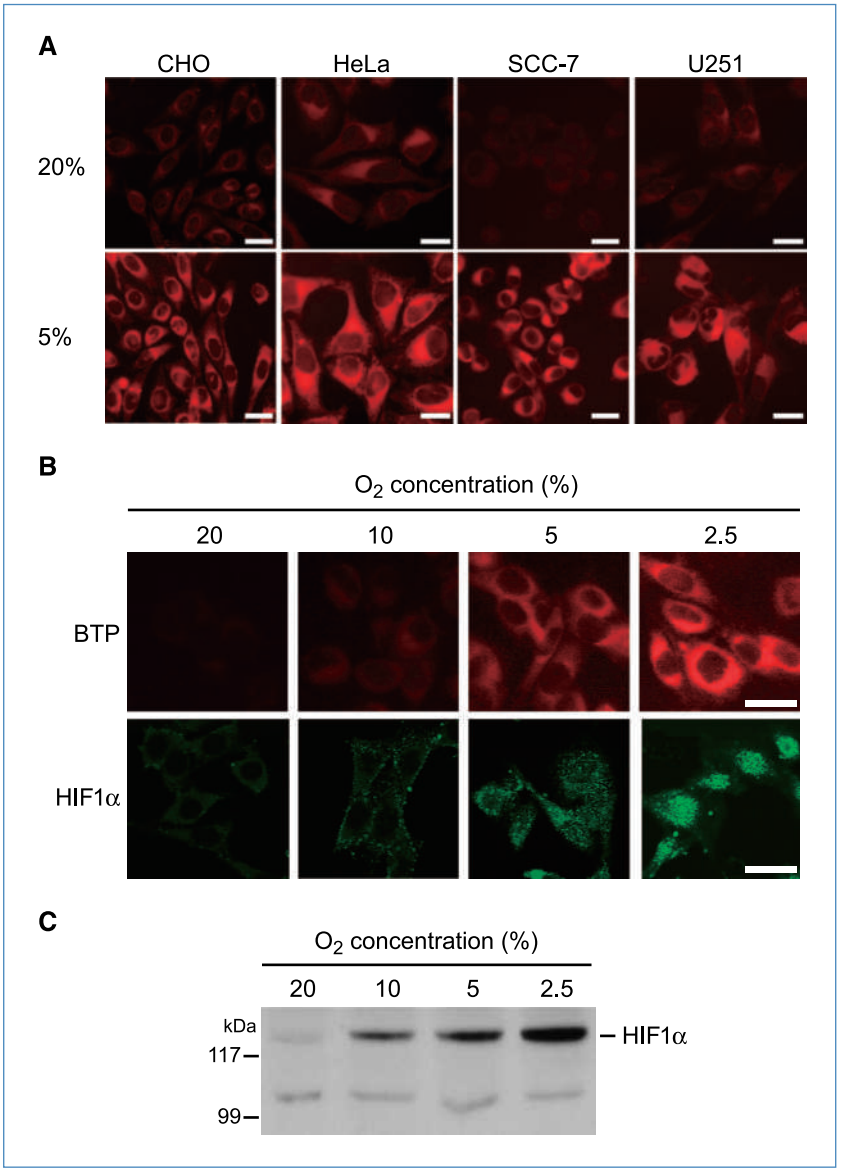

Figure 2. Cell imaging with BTP. A, BTP imaging of the four cell lines CHO, HeLa, SCC-7, and U251. The cells were cultured at 20% O_2 concentration (top) and 5% O_2 concentration (bottom). Scale bars, 10 μm. B, SCC-7 cells were placed at 20%, 10%, 5%, or 2.5% O_2 concentration. Top, BTP loading. Bottom, HIF-1α immunostaining. Scale bars, 10 μm. A and B, representative of six repeated experiments. C, Western blot of HIF-1α. SCC-7 cell lysates were subjected to SDS-PAGE after incubation with 20%, 10%, 5%, or 2.5% O_2 concentration.

be more concentrated in the nucleus than in the cytoplasm at 2.5% O_2 (Fig. 2B, bottom). In accordance with this, HIF-1α protein gradually displayed an intensive band (Fig. 2C).

Using the SCC-7 cells, we examined the uptake of BTP in the presence or absence of FBS or albumin in the culture medium. We added FBS or albumin to the SCC-7 culture medium for 2 hours then phosphorescence was evaluated under the fluorescent microscope. BTP or BTPHSA was poorly taken up into the cells in the absence of FBS or albumin. However, with the increase of FBS or albumin amounts in the culture medium, BTP analogues began to be taken up to the cells (Supplementary Fig. S1). Thus, BTP and its analogues are transported to the cells in an albumin-mediated manner and are released from albumin for their cellular uptake process.

BTP administration to tumor-bearing nude mice

For tumor imaging, we transplanted five culture cell lines into the lower thigh of nude mice: SCC-7, human glioma–derived U87, human lymphoma–derived RAMOS, human colon carcinoma–derived HT-29, and mouse lung cancer–derived LL-2. The tumor size varied from 10 to 15 mm. Tumors tended to show undifferentiated features, whose histopathology is described in Supplementary Fig. S2. With inserting an oxygen-monitoring probe 3- to 4-mm deep from the skin surface, we found that median pO_2 ranged from 18 to 21 mmHg (Supplementary Table S1). Thus, the pO_2 of each tumor was lower than that of end-capillary blood whose pO_2 ranges from 45 to 50 mmHg (2). We looked at HIF-1α immunostaining in the five tumors. HIF-1α was well stained in SCC-7 and in HT-29 tumors, but was not well noted in the other tumors (Supplementary Fig. S2).

We dissolved BTP in 10% DMSO due to its lipophilic feature. The BTP dose of 250 nmol/mouse was determined using SCC-7 tumor–bearing mice (data not shown). BTP (250 nmol/100 μL 10%DMSO) was injected from the tail vein under pentobarbital anesthesia. Each tumor-bearing mouse was placed in a dark box of the Maestro *In-Vivo* imaging System. Luminescence was detected 5 minutes after the injection in all five tumors and it increased gradually to a 1-hour point (Fig. 3). The shape and position of the luminescence spectra emitted from the tumors were identical with those of the BTP phosphorescence spectrum (Fig. 1B). Extratumor regions were virtually nonluminescent, but when anesthesia was overdosed, the forearm, perioral, and perinasal regions began to turn red. Furthermore, when the skin was pinched up and ligated with a thread, it became red within 1 minute after the ligation. Reversely, when the ligation was released, the skin turned to lose red-phosphorescence immediately (Supplementary Fig. S3A). Thus, BTP is distributed over the whole body and emits phosphorescence in which pO_2 decreases to a lower level.

We then determined the fate of BTP using SCC-7 tumors. The intensity of BTP was highest at 2 hours after the injection then declined gradually toward the 24-hours point when the tumor was not imaged (Supplementary Fig. S3B).

Detection limit of tumor size and imaging depth

We examined the detection limit of BTP-imaged tumor size. SCC-7 cells were injected into nude mice and their tumor size was monitored daily. When the tumor reached 1 mm or more in diameter, we began to assess BTP imaging. When a tumor grew to 2 mm in diameter, its BTP imaging was reliably detected (Supplementary Fig. S4A).

One of the drawbacks of luminescent imaging is the penetration limit of luminescence. We measured the penetration limit of BTP imaging by placing a 1.2-mm slice of pork ham on a BTP polyacrylamide gel. We could detect the BTP-imaging at a depth of 4.8 mm from the 20 nmol BTP gel and 7.2 mm from the 200 nmol BTP gel (Supplementary Fig. S4B, top). Because actual BTP content in the tumor ranges around 5 to 8 nmol/g (data not shown) and a lump of polyacrylamide gel is close to 1 g, the detection limit is presumed to be ~4 mm for BTP. Thus, to obtain much deeper tissue penetration, BTP should be modified for excitation by a red to near-IR wavelength.

***In vivo* imaging with a longer wavelength-shifted probe**

To shift the absorption and emission spectra to longer wavelengths, we synthesized BTPH (Fig. 4A), which has an extended π-electronic system compared with the benzothienyl-pyridinato group of the original BTP. Because the aqueous solubility of BTPH is extremely low, we further synthesized BTPHSA, a COOH derivative of BTPH (Fig. 4A), to improve the solubility. The first absorption maximum of BTPH and BTPHSA is located at ~550 nm and the phosphorescence maximum appears at 720 nm, i.e., in the near-IR region (Fig. 4A). It is noted that the phosphorescence quantum yield of BTPH and BTPHSA is still large (0.30 and 0.24, respectively, in degassed DCE).

We then measured the penetration limit of phosphorescence from BTPHSA, using a pile of ham slices. Because the concentrtion of BTPHSA in the tumor was ~3 nmol/g tumor weight, detection limit of phosphorescence seems to be ~10 mm from the surface (Supplementary Fig. S4B, bottom), which is deeper than that by BTP imaging. We

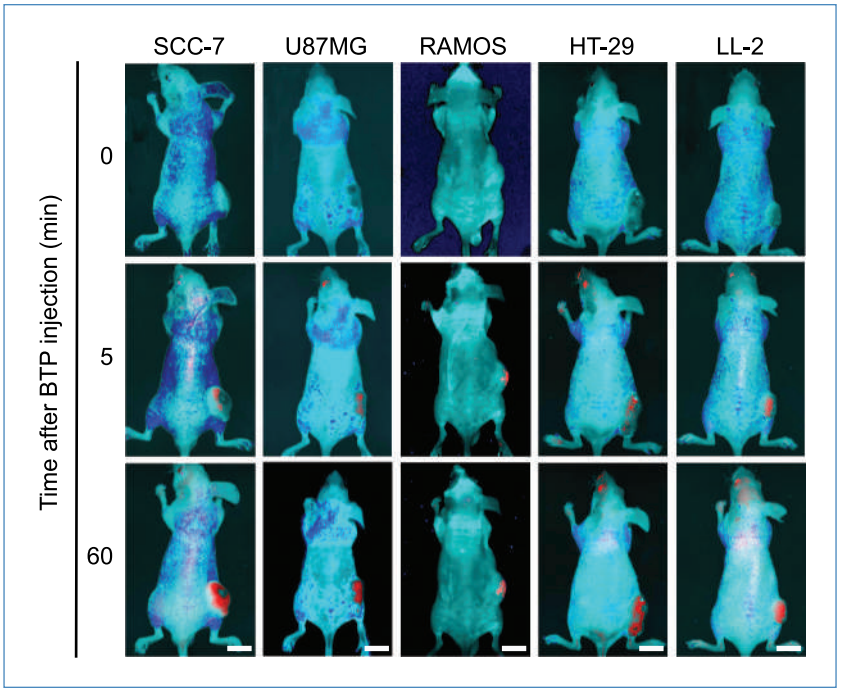

Figure 3. *In vivo* imaging with BTP. Tumor-bearing athymic nude mice were injected with 250 nmol BTP/100 μL DMSO from the tail vein. For BTP imaging, a tumor-bearing mouse was anesthetized by injecting pentobarbital (1.0 mg/mouse) i.p. The tumor image was obtained at 0, 5, and 60 min after the BTP injection. Scale bars, 10 mm.

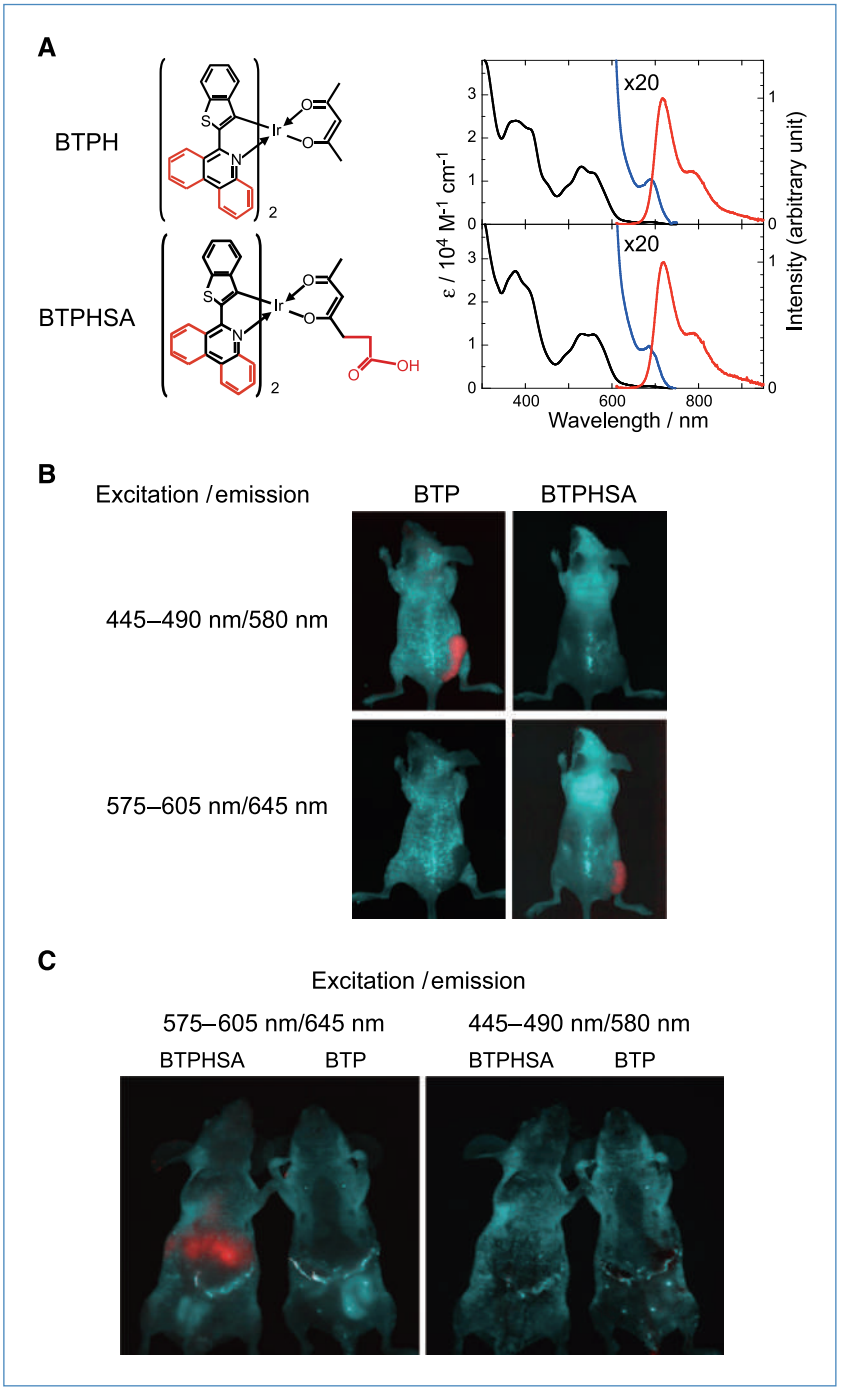

Figure 4. Imaging of BTPH with a longer excitation and emission wavelength. A, shift of excitation and emission to a longer wavelength range. Left, π-electron system–extended probes, BTPH and BTPHSA. Chemical structure was drawn with π-electron system–extended phenyl rings (red). Right, excitation [black line and its ×20 blow-up (blue)] and emission (red) spectra of BTPH and BTPHSA in DCE at room temperature. B, *in vivo* imaging for BTP- and BTPHSA-marked tumors. SCC-7 tumor was grown in the subcutaneous region. The tumor-bearing nude mice were injected with 250 nmol BTP or BTPHSA in a similar manner to the BTP-imaging experiment in Fig. 3. Phosphorescence was observed using Maestro for BTP and BTPHSA by excitation/emission of 445 to 490 nm/580 nm and 575 to 605 nm/645 nm. C, the detection depth with BTPHSA and BTP phosphorescence. SCC-7 tumors were excised and minced into pieces ~1 mm^3. The abdominal cavity was opened up and the backside of the liver was exposed. Four pieces of tumors were placed separately, 4 mm from each other, on the backside surface of the liver and were adhered by a surgical glue. The tumor sites were 6 to 7 mm deep from the abdominal skin surface. A week later, BTPHSA and BTP were injected from the tail vein and their phosphorescence images were taken by Maestro. Tumors were grown ~2 mm in diameter. Left, BTPHSA-marked tumors. Right, BTP-marked tumors. Filters were selected for BTPHSA and BTP as described in B.

next examined the detection wavelength for BTPHSA and BTP in subcutaneous SCC-7 tumor–bearing mice. The BTP-marked tumor was clearly visible by an excitation/emission wavelength of 445 to 490 nm/580 nm, whereas the BTPHSA-marked tumor was brightly imaged by 575 to 605 nm/645 nm (Fig. 4B). The maximal wavelength for BTP (615 nm) and for BTPHSA (720 nm) was longer than that used for this experiment. Thus, a combination of filter sets can be further improved. We lastly examined the detection depth of tumors *in vivo*. We removed and minced SCC-7 tumors into small pieces of ~1 mm^3, and then opened up the abdominal cavity under pentobarbital anesthesia and glued four pieces of tumors ~4 mm apart each other on the backside of the liver. A week later, we performed the phosphorescence imaging by BTPHSA and BTP. When we used an excitation/emission wavelength of 575 to 605 nm/645 nm, we could detect four BTPHSA phosphorescent images from the four tumors, although

each tumor image was a little fuzzy (Fig. 4C). BTP images were not detected. However, with 445 to 490 nm/580 nm, we could detect neither BTP nor BTPHSA image. The depth of tumor sites on the backside of the liver was measured 6 to 7 mm from the abdominal skin surface. Thus, we suggest that a longer wavelength-shifted BTP analogue improves the detection depth of tumors in living animals.

Tissue and cellular localization of BTP

In the first and second sections of Results, we assumed that BTP is transferred from albumin to the cells for its cellular uptake. To verify intracellular BTP localization, we used two methods: morphologic examination and phosphorescence lifetime measurement. For morphologic examination at the cellular level, we used HeLa cells culturing with 10% FBS. Cellular BTP localization seemed to be limited to the cytoplasm and not to the nucleus (Fig. 2B). We examined color merging using green-colored endoplasmic reticulum (ER)–specific probe ER tracker and mitochondria-specific probe Mitotracker. We observed a merged yellow color between BTP and ER tracker (Fig. 5A, top). However, no green-colored Mitotracker merged with BTP (Fig. 5A, bottom).

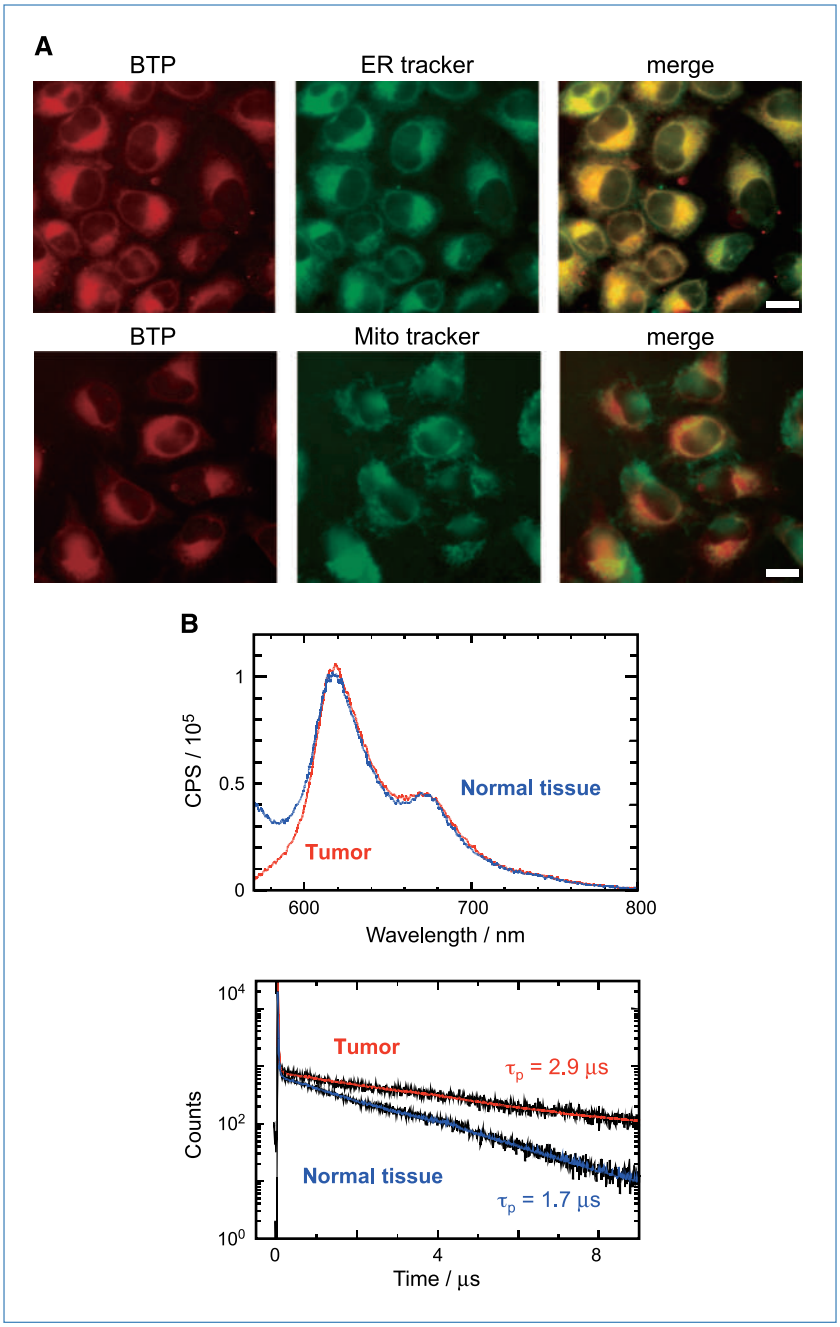

Figure 5. BTP localization in tumors. A, BTP localization in HeLa cells. BTP was added to the HeLa cell culture for 1 h at 5% O_2. Organelle markers used were ER tracker and Mito tracker, which selectively stain ER and mitochondria, respectively. Right, merged pictures. Scale bars, 10 μm. B, *in vivo* phosphorescence spectra and lifetime measurements. Top, phosphorescence spectra of BTP in tumors and normal tissues in a tumor-bearing nude mouse. Bottom, their decay curves monitored at 620 nm. The phosphorescence decay profiles could be fitted to single exponential functions with lifetimes of 2.9 and 1.7 μs, respectively, for the tumor moiety and the normal tissue.

Thus, BTP seems to have efficient access to the ER in the cytoplasm.

For tissue examination, we used the Olympus *in vivo* laser scanning microscope IV100. Initially, we applied this microscope to the tumor tissue, but could not detect a clear view, perhaps due to the less sensitive visualizing mechanism. However, after anesthetic death of the mouse, we could detect a relatively good view on the liver, which is the BTP excretion route to bile juice. BTP was indicated as green, whereas microvessels were marked with red AngioSense-750 (Supplementary Fig. S5). BTP appeared to be trapped in cell bodies, but it did not remain in microvessels and interstitial spaces. Thus, we suggest that BTP is transported to the cell bodies and is localized mostly to the ER.

Another method was performed with a phosphorescence lifetime measurement. The excitation light (337 nm) from a nanosecond-pulsed discharge lamp filled with nitrogen gas was collimated to the mouse tumor or normal tissues and the phosphorescence at 620 nm was detected by a photomultiplier tube after passing through a monochromator. The phosphorescence decay profiles could be fitted to single exponential functions with lifetimes of 2.9 and 1.7 μs for the tumor and the normal tissue, respectively (Fig. 5B). If we assume that BTP exists in the cell membrane, pO_2 for the tumor and the normal tissues can be evaluated to be 13 and 33 mmHg, respectively, using the k_q value (1.2×10^4 $mmHg^{-1}s^{-1}$) and τ_p^0 = 5.3 μs in the DMPC membrane. These values are consistent with those measured by an oxygen electrode (Supplementary Table S1). Judging from the extremely small quenching rate constant (5.0×10^2 $mmHg^{-1}s^{-1}$) for BTP bound to albumin, such a remarkable oxygen quenching will be impossible to occur if BTP exists binding to albumin in microvessels. Thus, we conclude that BTP is localized inside the cells and the longer lifetime of BTP in tumors than that in normal tissues clearly reflects a low oxygen concentration in the tumors.

Discussion

We showed a promising potential of the phosphorescent iridium complex, BTP analogues, for hypoxic tumor imaging. Using the oxygen-quenching feature, tumors were visible even 5 minutes after the BTP injection (Fig. 3). The luminescent region became widespread over the tumor profile 1 to 2 hours after the BTP injection and disappeared within 24 hours (Supplementary Fig. S3B). BTP analogues are distributed systemically to the whole body and emit phosphorescence where the oxygen supply is insufficient because simple skin ligation immediately displayed red phosphorescence (Supplementary Fig. S3A). In this sense, BTP analogues are distinct in its luminescence emission from other tumor-detecting probes, such as nitroimidazole, Cu(II)-ATSM, and ^{18}F-fluorodeoxyglucose. In other words, BTP analogues are hypoxia-sensing emitters, whereas the above three are hypoxia-accumulating emitters. For example, nitroimidazole accumulates in a hypoxic tissue in which the nitro residues are reduced by the lack of sufficient oxygen and the reduced form is thought to bind to macromolecules (6, 21). Cu(II)-ATSM is also reduced in hypoxic tissue to release Cu(I), which is thought to bind to macromolecules (22). These probes should be radiolabeled for PET and require cost-taking PET facilities and equipment.

Although BTP was distributed over the profile of a tumor (Fig. 3), it was questionable whether BTP is localized intracellularly to tumors or whether it stays in the tumor microvessels by binding to albumin. By morphologic examination and phosphorescence lifetime measurement, we found that BTP is localized to tumor cells, especially to ER organelles, and does not stay in the microvessels (Supplementary Fig. S5; Fig. 5). In this sense, BTP analogues are distinct from other phosphors such as dendrimer-coated porphyrins (14, 16, 23). BTP analogues are small phosphors with a molecular mass of 700 to 800 Da. In contrast, dendrimer-coated porphyrins are large in size, over 2 kDa, and remain in tumor microvessels or interstitial space without penetrating into cells (14, 16, 23).

Luminescent probes have an inevitable drawback, that is, their weak tissue penetration capacity, which is reportedly a magnitude of centimeters by near-IR wavelength light (24). The phosphorescence of BTP appears in the red to near-IR region (>600 nm), whereas the excitation wavelength is limited to the visible light region (445–490 nm). However, a great advantage of the iridium complexes lies in their facility in chemical modifications of the ligands. The ligand molecules of BTP consist of two benzothienyl-pyridinato groups and an acetylacetone as an ancillary ligand. The spectral properties of BTP are determined almost exclusively by the benzothienyl-pyridinato groups. On the other hand, the acetylacetone moiety in BTP analogues scarcely influences the spectral properties of the complex. We can, therefore, improve the absorption and emission properties of BTP to BTPH and BTPHSA by modifying this moiety (Fig. 4A). The penetration limit of BTPH was extended to ~1.0 mm deep (Supplementary Fig. S4B). Consistently, we were able to detect and count tumor numbers situated on the backside of the liver 6 to 7 mm deep from the abdominal skin surface (Fig. 4C). Thus, BTP imaging is applicable when tumors are situated relatively near the tissue surface such as gastrointestinal mucosal to submucosal layers. Because the detection limit of tumor size was estimated to be ~2 mm in diameter (Supplementary Fig. S4A), microadenoma and microcancer seem to be a target of BTP analogue imaging. We emphasize that BTP analogues are easily modified to better probes with a longer wavelength and appropriate water solubility. Furthermore, BTP analogues seem to be safe based on preliminary toxicity tests (data not shown). Therefore, we suggest that BTP analogues have practical feasibility for tumor hypoxia imaging.

Disclosure of Potential Conflicts of Interest

No potential conflicts of interest were disclosed.

Acknowledgments

We thank Dr. Chihaya Adachi (Kyushu University) and Dr. Ei-ichi Ozeki (Shimadzu BIOTECH) for their helpful discussion, Dr. Takashi Nakajima (Gunma University) for diagnosing histopathologic features of athymic

mouse transplanted with tumors, and Mari Kosaki and Mari Hosoi (Gunma University) for their secretarial and technical support.

Grant Support

Grants-in-Aid for Basic Sciences and a grant of the Global COE program from the Ministry of Education, Culture, Sports, Science and Technology of Japan, and by a Grant-in-Aid (Collaborative Development of Innovative Seeds) from Japan Science and Technology Agency.

The costs of publication of this article were defrayed in part by the payment of page charges. This article must therefore be hereby marked *advertisement* in accordance with 18 U.S.C. Section 1734 solely to indicate this fact.

Received 10/28/2009; revised 03/09/2010; accepted 03/15/2010; published OnlineFirst 05/11/2010.

References

1. Brahimi-Horn C, Berra E, Pouysségur J. Hypoxia: the tumor's gateway to progression along the angiogenic pathway. Trends Cell Biol 2001;11:S32–6.
2. Höckel M, Vaupel P. Tumor hypoxia: definitions and current clinical, biologic, and molecular aspects. J Natl Cancer Inst 2001;93:266–76.
3. Ryan HE, Poloni M, McNulty W, et al. Hypoxia-inducible factor-1α is a positive factor in solid tumor growth. Cancer Res 2000;60:4010–5.
4. Schofield CJ, Ratcliffe PJ. Oxygen sensing by HIF hydroxylases. Nat Rev Mol Cell Biol 2004;5:343–54.
5. Nunn A, Linder K, Strauss HW. Nitroimidazoles and imaging hypoxia. Eur J Nucl Med 1995;22:265–8.
6. Padhani AR, Lrohn KA, Lewin JS, et al. Imaging oxygenation of human tumours. Eur Radiol 2007;17:861–72.
7. Maurer RI, Blower PJ, Dilworth JR, et al. Studies on the mechanism of hypoxic selectivity in copper bis(thiosemicarbazone) radiopharmaceuticals. J Med Chem 2002;45:1420–31.
8. Mankoff DA, Eary JF, Link JM, et al. Tumor-specific positron emission tomography imaging in patients: [^{18}F] fluorodeoxyglucose and beyond. Clin Cancer Res 2007;13:3460–9.
9. Wilson DF, Vinogradov SA. Tissue oxygen measurements using phosphorescence quenching. In: Mycek M-A, Pogue BW, editors. Handbook of Biomedical Fluorescence. New York: Marcel Dekker, Inc.; 2003. p. 637–62.
10. Dobrucki JW. Interaction of oxygen-sensitive luminescent probes Ru(phen)$_3^{2+}$ and Ru(bipy)$_3^{2+}$ with animal and plant cells *in vitro*: mechanism of phototoxicity and conditions for non-invasive oxygen measurements. J Photochem Photobiol 2001;65:136–44.
11. Morris KL, Roach MS, Xu W, et al. Luminescence lifetime standards for the nanosecond to microsecond range and oxygen quenching of Ruthenium(II) complexes. Anal Chem 2007;79:930–14.
12. DeRosa MC, Mosher PJ, Yap GPA, et al. Synthesis, characterization, and evaluation of [Ir(ppy)$_2$(vpy)Cl] as a polymer-bound oxygen sensor. Inorg Chem 2003;42:4864–72.
13. Vinogradov SA, Lo L-W, Jenkins WT, et al. Noninvasive imaging of the distribution in oxygen in tissue *in vivo* using near-infrared phosphors. Biophys J 1996;70:1609–17.
14. Ziemer LS, Lee WMF, Vinogradov SA, et al. Oxygen distribution in murine tumors: characterization using oxygen-dependent quenching of phosphorescence. J Appl Physiol 2005;98:1503–10.
15. Babilas P, Liebsch G, Schacht V, et al. *In vivo* phosphorescence imaging of pO_2 using planar oxygen sensors. Microcirculation 2005;12:477–87.
16. Dunphy I, Vinogradov SA, Wilson DF. Oxyphor R2 and G2: phosphors for measuring oxygen by oxygen-dependent quenching of phosphorescence. Anal Biochem 2002;310:191–8.
17. Briñas RP, Troxier T, Hochstrasser RM, et al. Phosphorescent oxygen sensor with dendritic protection and two-photon absorbing antenna. J Am Chem Soc 2005;127:11851–62.
18. Jorge PAS, Maule C, Silva AJ, et al. Dual sensing of oxygen and temperature using quantum dots and a ruthenium complex. Anal Chim Acta 2008;606:223–9.
19. Lamansky S, Djurovich P, Murphy D, et al. Highly phosphorescent bis-cyclometalated iridium complexes: synthesis, photophysical characterization, and use in organic light emitting diodes. J Am Chem Soc 2001;123:4304–12.
20. Lakowicz JR. Quenching of Fluorescence. In Principles of Fluorescence Spectroscopy. 3rd Edition. New York: Springer; 2006. pp. 277–330.
21. Varghese AJ, Gulyas S, Mohindra JK. Hypoxia-dependent reduction of 1-(2-nitro-1-imidazolyl)-3-methoxy-2-propanol by Chinese hamster ovary cells and KHT tumor cells *in vitro* and *in vivo*. Cancer Res 1976;36:3761–5.
22. Lewis JS, Herrero P, Sharp TL, et al. Delineation of hypoxia in canine myocardium using PET and copper(II)-diacetyl-bis(N(4)-methylthiosemicarbazone). J Nucl Med 2002;43:1557–69.
23. Wilson DF, Lee WMF, Makonnen S, et al. Oxygen pressures in the interstitial space and their relationship to those in the blood plasma in resting skeletal muscle. J Appl Physiol 2006;101:1648–56.
24. Kaijzel EL, van der Pluijm G, Löwik GCW. Whole-body optical imaging in animal models to assess cancer development and progression. Clin Cancer Res 2007;13:3490–7.